Review of Scientific Instruments

X-ray backlighter requirements for refraction-based electron density diagnostics through Talbot-Lau deflectometry

Cite as: Rev. Sci. Instrum. **89**, 10G127 (2018); https://doi.org/10.1063/1.5039342
Submitted: 07 May 2018 . Accepted: 08 September 2018 . Published Online: 25 October 2018

M. P. Valdivia, F. Veloso, D. Stutman, C. Stoeckl, C. Mileham, I. A. Begishev, W. Theobald, M. Vescovi, W. Useche, S. P. Regan, B. Albertazzi, G. Rigon, P. Mabey, T. Michel, S. A. Pikuz, M. Koenig, and A. Casner

X-ray backlighter requirements for refraction-based electron density diagnostics through Talbot-Lau deflectometry

M. P. Valdivia,[1,a)] F. Veloso,[2] D. Stutman,[1] C. Stoeckl,[3] C. Mileham,[3] I. A. Begishev,[3] W. Theobald,[3] M. Vescovi,[2] W. Useche,[2] S. P. Regan,[3] B. Albertazzi,[4] G. Rigon,[4] P. Mabey,[4] T. Michel,[4] S. A. Pikuz,[5] M. Koenig,[4] and A. Casner[6]

[1]*Department of Physics and Astronomy, Johns Hopkins University, Baltimore, Maryland 21218, USA*
[2]*Instituto de Física, Pontificia Universidad Católica de Chile, Casilla 306, Santiago, Chile*
[3]*Laboratory for Laser Energetics, University of Rochester, Rochester, New York 14623, USA*
[4]*Laboratoire pour l'Utilisation de Lasers Intenses, CNRS CEA, Ecole Polytechnique, 91128 Palaiseau Cedex, France*
[5]*Joint Institute for High Temperatures, Russian Academy of Sciences, Moscow 125412, Russia*
[6]*Université de Bordeaux-CNRS-CEA, CELIA, UMR 5107, F-33405 Talence, France*

(Presented 17 April 2018; received 7 May 2018; accepted 8 September 2018; published online 25 October 2018)

Talbot-Lau x-ray interferometers can map electron density gradients in High Energy Density (HED) samples. In the deflectometer configuration, it can provide refraction, attenuation, elemental composition, and scatter information from a single image. X-ray backlighters in Talbot-Lau deflectometry must meet specific requirements regarding source size and x-ray spectra, amongst others, to accurately diagnose a wide range of HED experiments. 8 keV sources produced in the high-power laser and pulsed power environment were evaluated as x-ray backlighters for Talbot-Lau x-ray deflectometry. In high-power laser experiments, K-shell emission was produced by irradiating copper targets ($500 \times 500 \times 12.5\ \mu m^3$ foils, 20 μm diameter wire, and >10 μm diameter spheres) with 30 J, 8-30 ps laser pulses and a 25 μm copper wire with a 60 J, 10 ps laser pulse. In the pulsed power environment, single ($2 \times 40\ \mu m$) and double ($4 \times 25\ \mu m$) copper x-pinches were driven at ~1 kA/ns. Moiré fringe formation was demonstrated for all x-ray sources explored, and detector performance was evaluated for x-ray films, x-ray CCDs, and imaging plates in context of spatial resolution, x-ray emission, and fringe contrast. *Published by AIP Publishing.* https://doi.org/10.1063/1.5039342

I. INTRODUCTION

A. Talbot-Lau x-ray deflectometry (TXD)

Talbot-Lau x-ray deflectometry is a single-shot diagnostic variation of the Talbot-Lau interferometer.[1,2] It facilitates quantitative analysis of electron density in plasmas where refractive index changes produce angular deviations of probing beams, which are proportional to electron density gradients.[3] In recent years, TXD adaptations have been studied to map electron density in High Energy Density (HED) experiments, particularly for Inertial Confinement Fusion (ICF),[4] since it can additionally diagnose micro-instabilities and mixing, for example.[5] The small features in the dense fuel found at peak compression in ICF experiments require spatial resolutions of <10 μm. Moreover, temporal resolutions of <10 ps are necessary to image high-speed fuel burn avoiding motion blurring.[6]

Talbot-Lau interferometers are designed for optimum performance at a specific energy, determined by a contrast curve given by grating characteristics and the spectral bandwidth ($\Delta E/E$) which is proportional to the inverse of the Talbot order.[1,2,7] Therefore, x-ray backlighter sources can have relatively broad spectra. Typically, low orders (m = 1-5) are utilized. Furthermore, at high Talbot magnification $M_T = L + D/L \gg 1$ (with L source grating to phase grating distance and D phase grating to analyzer grating distance), the electron density gradient resolution depends on the grating period and spectral bandwidth. Namely, the refraction angle of an x-ray beam passing through a medium with electron density gradients will be given by

$$\alpha(x \cdot y) = \frac{\lambda^2 r_e}{2\pi} \frac{\partial}{\partial x} \int N_e(x, y, z) dz, \tag{1}$$

where α is the angular refraction, λ is the probing beam wavelength, r_e is the classical electron radius, and N_e is the electron density.

TXD integrates along the beam direction, in similarity to standard radiography[8] and interferometry[9] diagnostics, thus delivering line integrated electron density information. Nevertheless, elemental composition diagnostic capabilities of TXD can compensate for this.[10]

The refraction angle obtained through TXD is given by grating periods, object to source grating distance, and Moiré fringe shift measured. By simplifying,

$$\alpha \approx W_{\text{eff}} F = \frac{g_0}{P} F, \tag{2}$$

where W_{eff} is the angular sensitivity (g_0/P),[4] F is the fringe shift, g_0 is the source grating period, and P is the object to source grating distance.

Note: Paper published as part of the Proceedings of the 22nd Topical Conference on High-Temperature Plasma Diagnostics, San Diego, California, April 2018.

a)Author to whom correspondence should be addressed: mpvaldivia@pha.jhu.edu

B. High energy density x-ray backlighters

HED x-ray backlighters can be produced through laser-target interaction and from x-pinch discharges. These x-ray sources were explored, and their performance in the context of Talbot-Lau deflectometry was tested. Typically, in the high-intensity laser environment, <1 mm^2 foils with thicknesses of a few to hundreds of microns are irradiated with laser pulses of ~10^{18} W/cm^2. This produces K-shell and He-like x-ray emission in the range of ~1-100 keV, depending on target material.[11,12] Similarly, in the pulsed power environment, x-pinch discharges can produce point sources in the same energy range.[13] This emission originates from the highly dense cross-point once compression conditions are met,[14] which often translates to ratios of maximum current to rise time of >1 kA/ns.

C. X-ray backlighter requirements

1. Timing

In the laser environment, x-ray backlighter time resolution is given by laser pulse duration, typically in the range of a few ps to tens of ns.[15] Nevertheless, pulse-dilation techniques are known to achieve improved temporal resolution.[16] In the case of pulsed power, x-pinch hotspot emission is typically <1 ns,[14,17] and it depends on current pulse characteristics. In this case, time resolution can be improved pulse dilated systems, for example.

2. Source size

In TXD, spatial resolution is given by the source size, object magnification, and detector characteristics. It is equivalent to the resolution expected from a conventional radiographic system. Nevertheless, if the source size is much larger than the source grating period, the spatial resolution is improved due to the Lau effect along the fringes.[18] Perpendicular to the fringes, the resolution has been shown to be equal or better than half a fringe period (projected at the object location).[4]

3. Spectrum

Backlighter spectrum impacts electron density detection [Eq. (1)] as it relates to measurement error due to spectral bandwidth. To achieve optimum contrast, gratings are placed at specific locations where intensity is maximum, known as the Talbot distance,

$$d_T = \frac{g^2}{8\lambda} m, \tag{3}$$

where g is the grating period and m is the Talbot order.

Talbot-Lau interferometer contrast is defined as the differential ratio of maximum and minimum intensities: $V = (I_{max} - I_{min})/(I_{max} + I_{min})$. Total intensity measured at a specific point in space [Eq. (3)] is composed of all intensities produced by the energy bandwidth from the probing x-ray beam. Since TXD systems are designed to work optimally under a specific illumination energy by fixing inter-grating distances, broad spectra decreases contrast. For the TXD configurations studied and presented, low contrast does not affect electron density retrieval accuracy beyond measurement uncertainty [$\Delta\lambda$ in Eq. (1)]. However, low contrast Moiré images negatively impacts phase-retrieval through Fourier methods. In the laboratory, it has been shown that contrast of ~10% is enough to accurately retrieve electron densities with errors of <5%.[19] From Eqs. (1) and (2), it can be inferred that the electron density range that can be measured by an 8 keV TXD system with a 2.4 μm source grating is ~1% to a few times solid density.

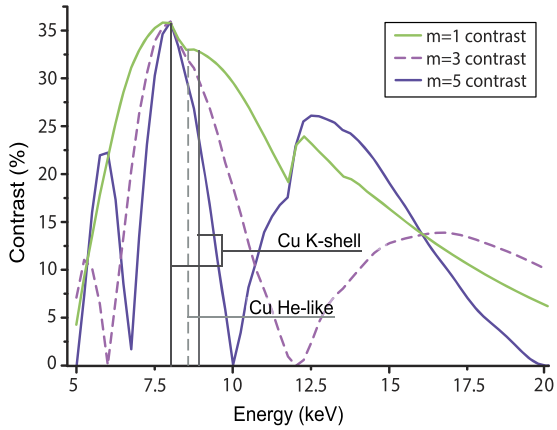

FIG. 1. Simulated contrast curves for the 8 keV Talbot-Lau interferometer studied. Talbot orders: m = 1, 3, 5, were obtained from XWFP code.[20] Expected Cu emission lines are shown as well.

Since interferometer contrast is highly dependent on the spectrum,[4] an excess of x-ray energies outside the contrast bandwidth chosen will decrease Moiré fringe contrast. For instance, 12.5 keV photons produce 25% Moiré fringe contrast in the m = 5 configuration tested, whereas for 8 keV photons, the contrast is 35% (Fig. 1). For TXD systems composed of gold gratings (~10-100 μm thickness), 12.5 keV photons have transmissivities nearly five times larger than 8 keV photons for each grating. While lower energies can be filtered easily, higher energies present a challenge. Higher energies can be minimized using a detector with rapidly decaying gain at higher x-ray energies.

II. EXPERIMENTAL CONFIGURATION

A. High-power laser x-ray backlighters

The TXD systems studied were composed of three micro-gratings, as shown in Fig. 2(a). The specifics of these gratings can be found in Ref. 19. Two TXD configurations were tested in high-power laser experiments. The first experiment was performed in the Multi-TeraWatt (MTW) single-beam laser facility[21,22] where laser pulses of <30 J, 8-30 ps were focused on $500 \times 500 \times 12.5$ μm^3 Cu foil targets and CH-backed Cu targets: wires of 20 μm diameter and 14-35 μm diameter spheres. Due to target chamber restrictions, a Talbot order of m = 3 was chosen and an angular refraction sensitivity of ~80 μrad was achieved with P = 3 cm [Eq. (2)].[5,23] Moiré deflectometry images were recorded using an x-ray CCD camera (Andor iKon-M) with 13 μm pixels with an object magnification of ~9. A Highly Oriented Pyrolytic Graphite (HOPG) crystal spectrometer detected x-ray emission in the 8 keV range. The second TXD test was carried out in the LULI laser facility as a ride-along diagnostic in astrophysically relevant plasma

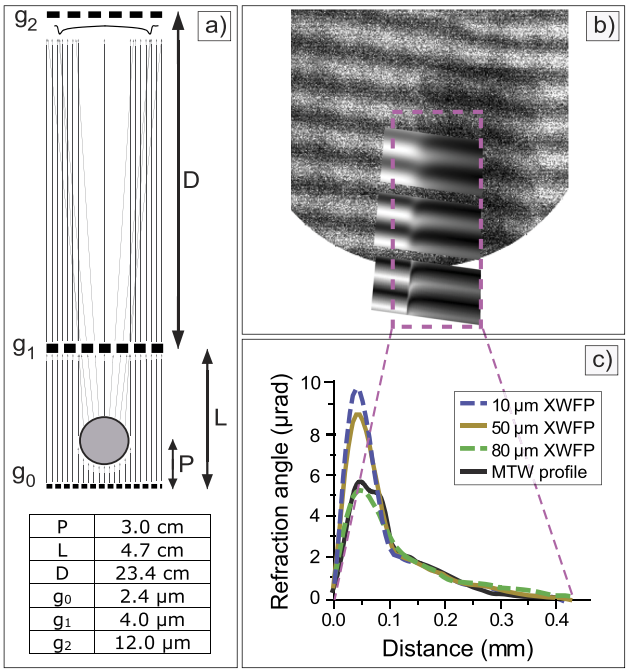

FIG. 2. (a) Schematic of TXD setup at MTW. (b) Moiré image of a 750 μm diameter acrylic rod. (c) Refraction angle profiles obtained through TXD: simulations of 80, 50, and 10 μm source sizes and MTW experimental data.

experiments driven by a 1 kJ, 1.5 ns laser pulse. For TXD backlighting, a 25 μm Cu wire was driven by the PICO2000 laser at 60 J, 10 ps to generate 8 keV x-rays. Based on plasma target location and chamber geometry, a Talbot order of m = 5 was chosen (L = 7.7 cm and D = 38.7 cm) with P = 1.2 cm. The angular sensitivity achieved was $W_{eff} \sim 200$ μrad. Radiography and deflectometry images of static objects were recorded using an imaging plate with magnifications ~3-9 in order to benchmark backlighter performance.

B. Pulsed power x-ray backlighter

X-ray emission was obtained from single (2 × 40 μm) and double (4 × 25 μm) copper x-pinch loads driven at ~400 kA, ~1 kA/ns.[24] A Talbot order of m = 1 was chosen, and the TXD platform was set 6.5 cm away from the x-pinch cross-point, restricted by the high magnetic field zone and taking into account the vacuum chamber geometry. The x-ray emission spectrum was determined using x-ray diodes with Ross-pair filters (Al, Ni, and Fe). A static test object was placed 0.5 cm behind the phase grating rotation stage, which led to an angular sensitivity of $W_{eff} \sim 240$ μrad. Moiré images were recorded on the Carestream D-Speed x-ray film placed directly behind the analyzer grating rotation stage with an object magnification of ~2.

III. X-RAY BACKLIGHTER PERFORMANCE

A. Laser backlighter

At MTW, foil backlighters shot at 45° provided a spatial resolution of ~50 μm obtained through knife-edge measurements (10%-90% rise method). Since the desired resolution in ICF is <10 μm, CH backed micro-targets pursued source sizes to match the required <10 μm: 20 μm wires and 14-25 μm spheres achieved spatial resolutions of <40 and <25 μm, respectively. Similarly, a 25 μm stand-alone wire delivered a spatial resolution of ~25 μm in the LULI system. The spatial resolution values obtained are directly related to the laser spot size, detector characteristics, target orientation, and target dimension.[25]

Figure 2(b) shows a Moiré image of a 750 μm acrylic rod obtained at MTW with a 28 J, 30 ps laser pulse. Simulations of 80, 50, and 10 μm x-ray sources are overlaid. It can be inferred that source size is close to 80 μm, corroborated by knife-edge measurements.[5] Fourier processing of Moiré images delivers the refraction angle as determined by Eq. (2). The traces in Fig. 2(c) illustrate spatial resolution impact on angular resolution achieved through phase-retrieval methods. Larger sources resolve up to 5 μrad due to gauss broadening, while smaller sources are able to resolve up to 10 μrad, still far from the maximum detectable angle of 80 μrad given by system parameters. Therefore, smaller source sizes are required to optimize electron density mapping.

Figure 3 shows HOPG spectra recorder for foil and wire targets. K-shell emission was measured for all targets studied in the MTW laser system. This included the K-alpha lines at 8.03 and 8.05 keV as well as the K-beta line at 8.91 keV. In the case of micro-targets, He-like emission was also measured at 8.35 keV.

The emission lines fall under the optimum TXD contrast curve (Fig. 1). The He-like line falls between K-shell lines and is exclusive to micro-targets. All targets investigated have the same energy bandwidth, and thus, the same electron density resolution range. Laser-target interactions often produce hot electrons, which generate higher emission than the desired K-shell lines.[26] In particular, micro-backlighters show evidence of emission of higher energy due to electron recirculation,[27] which lowers overall contrast. This is evident from the measurements of ~15%-25% contrast for foil targets as well as 7%-17% for wire and sphere targets.[5] By contrast, a maximum of 30% was achieved in the laboratory when imaging test objects using the same interferometer setup.

For the second laser experiment, performed at LULI, a short pulse laser irradiated wire targets delivering 8 keV emission with 25 μm spatial resolution, consistent with MTW observations. In this experiment, the main goal was to demonstrate Moiré fringe formation and grating survival first in the presence of a backlighter and then in the presence of a plasma object. An average fringe contrast below 5% was recorded even in the absence of plasma target, as shown in Fig. 4. In the laboratory, using the XRCCD from MTW experiments, the contrast achieved was close to 22%. The low value measured is thus attributed to the detector. Unlike the x-ray CCD used in MTW experiments, imaging plates are able to efficiently record higher energy emission and thus, fringe contrast was severely compromised. Since CCDs can be affected by system EMPs, imaging plate performance was explored in these studies, nevertheless, it was shown that they are not the best alternative when using low energy (1-10 keV) backlighters.

It should be noted that, due to high self-emission, gold grid radiography images recorded in the presence of plasma object

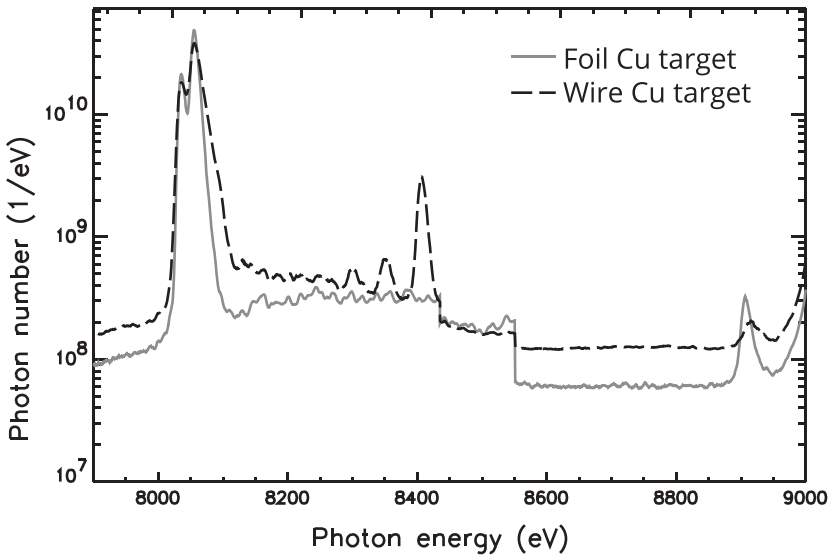

FIG. 3. HOPG spectra for MTW experiments: (a) foils and (b) wires.

delivered lower contrast and spatial resolution, in comparison with images without plasma. Consequently, and considering the low contrast achieved without target, no Moiré patterns were recorded with a plasma target. Therefore, no spatial resolution or density gradient maps were obtained during the first experimental run at LULI.

B. X-pinch backlighters

The pulsed power TXD setup uses the same gratings from laser experiments in the m = 1 configuration (L = 1.6 cm and D = 7.8 cm) and has been described in detail previously.[5] Source sizes were measured through slit-wire imaging,[28] delivering FWHM of <50 and <27 μm for single (2 × 40 μm) and double (4 × 25 μm) Cu x-pinches, respectively. While these source sizes coincide with cross-point dimensions, potentially smaller sources could be achieved with better hotspot compression through current pulse modification. If x-pinch loads are not properly matched to the generator impedance, multiple hotspots (and sources) are expected. From filtered diode signals, it was found that both x-pinch loads emit in the 8 keV range. Considering the ionization states expected for these x-pinch discharges, K-alpha emission (and no He-like) should be present. This was confirmed by filtered x-ray diodes. A low contrast value of ~14% was measured (Fig. 5), compared to the 33% contrast obtained in the laboratory using a continuum x-ray source in combination with an x-ray CCD.[19] This low contrast could be due to additional emission of lines outside the optimal contrast curve or from Bremsstrahlung emission from electron beams. It is also likely that, in similarity with imaging plates, the detector gain is an important factor. Due to the chamber and EMP restrictions, the x-ray film was chosen to record Moiré images. However, the film is not optimum considering TXD design energy. The x-ray film is designed for x-rays above 20 keV, with low gain for lower energies. Furthermore, since x-pinch emission flux is known to be lower than laser-target interactions, detector performance and gain should be optimized.[29,30]

A beryllium sheet of 1.0 × 0.5 × 0.1 cm^3, chosen based on the system geometry, was placed at a small angle so that the sheet edges act as deflection prisms. Fringe shift from refraction was observed along with x-ray attenuation (Fig. 5). It should be noted that the x-ray film image presented is the negative of the Moiré image, that is, the lighter sections correspond to the largest attenuation. As expected in this geometry, no fringe shift is observed on both sides of the film: On the left, in and out x-ray beam angles are equal, and on the right, there is no object. Angular refraction was retrieved with ~6% error when compared to the theoretical value. It is worth noting that grating imperfections, as described in Ref. 19, are visible due to higher spatial resolution achieved with x-pinch backlighters.

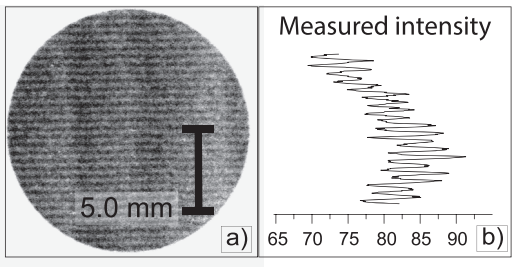

FIG. 4. (a) Moiré pattern recorded with an imaging plate at LULI. Scaling measured at object plane and contrast enhanced to show fringe pattern. (b) Measured intensity plot.

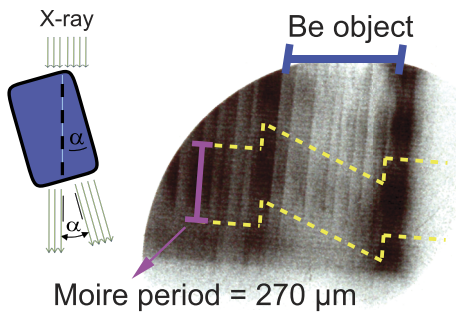

FIG. 5. Be sheet Moiré image from Cu x-pinches driven at ~1 kA/ns.

IV. SUMMARY

The x-ray backlighter configurations explored exhibit time resolutions of a few ps, close to that expected from the laser pulse in the case of laser-target interactions. Similarly, x-pinch emission was measured to be <1 ns, limited by detector rise time. When evaluating spatial resolution requirements for x-ray backlighters, source sizes from x-pinches are smaller than those measured in laser-target experiments. Notably, micro-targets were found to produce sources with improved spatial resolution, nevertheless, these targets also emit harder radiation which negatively impacts fringe contrast. This can be addressed, for example, by combining the system with refractive optics selecting the appropriate x-ray energy.[31] Additionally, emission due to hot electron recirculation can be mitigated through laser pulse and target modification. Both these approaches will be explored in future studies.

X-ray emission from laser-based x-ray backlighters delivered photon flux well above the minimum required by the detector in contrast to the x-pinch x-ray sources explored. Due to low photon flux, x-ray film developing had to be modified in order to record a Moiré image that could be digitally processed. Generally, to optimize x-ray backlighters, the x-ray detector must have high gain for 8 keV photons and low gain for higher energy photons. Both x-ray backlighters studied emitted ~8 keV x-rays, corresponding mostly to copper K-shell emission. In the case of micro-backlighters, He-like emission was detected while higher energies due to electron recirculation effects are evident from low fringe contrast. Low contrast was also observed in experiments using imaging plate detectors as well as hard x-ray films. The use of specific x-ray detectors with quantum efficiencies that rapidly decay with increasing x-ray energy, such as XRCCDs, can aid in interferometer contrast optimization.

The results presented show that x-ray sources generated in two different HEDP environments can deliver suitable x-ray backlighters for TXD refraction based diagnostics. Recommendations for x-ray backlighter optimization have been outlined, indicating that TXD could be a powerful refraction diagnostic tool for HEDP experiments in the high-power laser and pulsed power environments.

ACKNOWLEDGMENTS

The authors would like to thank S. R. Klein for providing the micro-targets used in these studies and G. Muñoz-Cordovez and V. Valenzuela-Villaseca for their scientific and technical support. M. Vescovi acknowledges CONICYT scholarship for graduate studies. This work was supported by U.S. DOE under NNSA Grant Nos. DE-NA0002955 and FONDECYT/Regular 1171412.

[1]F. Pfeiffer, T. Weitkamp, O. Bunk, and C. David, Nat. Phys. **2**, 258 (2006).
[2]A. Momose, W. Yashiro, Y. Takeda, Y. Suzuki, and T. Hattori, Jpn. J. Appl. Phys., Part 1 **45**, 5254 (2006).
[3]D. Stutman and M. Finkenthal, Rev. Sci. Instrum. **82**, 113508 (2011).
[4]M. P. Valdivia, D. Stutman, and M. Finkenthal, J. Appl. Phys. **114**, 163302 (2013).
[5]M. P. Valdivia, D. Stutman, C. Stoeckl, C. Mileham, I. A. Begishev, W. Theobald, J. Bromage, S. P. Regan, S. R. Klein, G. Muñoz-Cordovez, M. Vescovi, V. Valenzuela-Villaseca, and F. Veloso, Rev. Sci. Instrum. **87**, 11D501 (2016).
[6]R. Tommasini, A. MacPhee, D. Hey, T. Ma, C. Chen, N. Izumi, W. Unites, A. MacKinnon, S. P. Hatchett, B. A. Remington, H. S. Park, P. Springer, J. A. Koch, O. L. Landen, J. Seely, G. Holland, and L. Hudson, Rev. Sci. Instrum. **79**, 10E901 (2008).
[7]H. F. Talbot, London, Edinburgh, Dublin Philos. Mag. J. Sci. **9**, 401 (1836).
[8]E. Brambrink, S. Baton, M. Koenig, R. Yurchak, N. Bidaut, B. Albertazzi, J. E. Cross, G. Gregori, A. Rigby, E. Falize, A. Pelka, F. Kroll, S. Pikuz, Y. Sakawa, N. Ozaki, C. Kuranz, M. Manuel, C. Li, P. Tzeferacos, and D. Lamb, High Power Laser Sci. Eng. **4**, e30 (2016).
[9]G. F. Swadling, S. V. Lebedev, N. Niasse, J. P. Chittenden, G. N. Hall, F. Suzuki-Vidal, G. Burdiak, A. J. Harvey-Thompson, S. N. Bland, P. De Grouchy, E. Khoory, L. Pickworth, J. Skidmore, and L. Suttle, Phys. Plasmas **20**, 022705 (2013).
[10]M. P. Valdivia, D. Stutman, and M. Finkenthal, Appl. Opt. **54**, 2577 (2015).
[11]F. N. Beg, A. R. Bell, A. E. Dangor, C. N. Danson, A. P. Fews, M. E. Glinsky, B. A. Hammel, P. Lee, P. A. Norreys, and M. Tatarakis, Phys. Plasmas **4**, 447 (1997).
[12]D. Riley, N. C. Woolsey, D. McSherry, F. Y. Khattak, and I. Weaver, Plasma Sources Sci. Technol. **11**, 484 (2002).
[13]T. A. Shelkovenko, D. B. Sinars, S. A. Pikuz, K. M. Chandler, and D. A. Hammer, Rev. Sci. Instrum. **72**, 667 (2001).
[14]M. G. Haines, Plasma Phys. Controlled Fusion **53**, 093001 (2011).
[15]H. S. Park, D. M. Chambers, H. K. Chung, R. J. Clarke, R. Eagleton, E. Giraldez, T. Goldsack, R. Heathcote, N. Izumi, M. H. Key, J. A. King, J. A. Koch, O. L. Landen, A. Nikroo, P. K. Patel, D. F. Price, B. A. Remington, H. F. Robey, R. A. Snavely, D. A. Steinman, R. B. Stephens, C. Stoeckl, M. Storm, M. Tabak, W. Theobald, R. P. J. Town, J. E. Wickersham, and B. B. Zhang, Phys. Plasmas **13**, 056309 (2006).
[16]S. R. Nagel, T. J. Hilsabeck, P. M. Bell, D. K. Bradley, M. J. Ayers, K. Piston, B. Felker, J. D. Kilkenny, T. Chung, B. Sammuli, and J. D. Hares, Rev. Sci. Instrum. **85**, 11E504 (2014).
[17]S. A. Pikuz, T. A. Shelkovenko, D. B. Sinars, and D. A. Hammer, Plasma Phys. Rep. **32**, 1020 (2006).
[18]J. Jahns and A. W. Lohmann, Opt. Commun. **28**, 263 (1979).
[19]M. P. Valdivia, D. Stutman, and M. Finkenthal, Rev. Sci. Instrum. **85**, 073702 (2014).
[20]T. Weitkamp, Proc. SPIE **5536**, 181 (2004).
[21]V. Bagnoud, I. A. Begishev, M. J. Guardalben, J. Puth, and J. D. Zuegel, Opt. Lett. **30**, 1843 (2005).
[22]C. Dorrer, I. A. Begishev, A. V. Okishev, and J. D. Zuegel, Opt. Lett. **32**, 2143 (2007).
[23]M. P. Valdivia, D. Stutman, C. Stoeckl, W. Theobald, C. Mileham, I. A. Begishev, J. Bromage, and S. P. Regan, Rev. Sci. Instrum. **87**, 023505 (2016).
[24]H. Chuaqui, E. Wyndham, C. Friedli, and M. Favre, Laser Part. Beams **15**, 241–248 (1997).
[25]H. S. Park, B. R. Maddox, E. Giraldez, S. P. Hatchett, L. T. Hudson, N. Izumi, M. H. Key, S. Le Pape, A. J. MacKinnon, A. G. MacPhee, P. K. Patel, T. W. Phillips, B. A. Remington, J. F. Seely, R. Tommasini, R. Town, J. Workman, and E. Brambrink, Phys. Plasmas **15**(7), 072705 (2008).
[26]P. M. Nilson, A. A. Solodov, J. F. Myatt, W. Theobald, P. A. Jaanimagi, L. Gao, C. Stoeckl, R. S. Craxton, J. A. Delettrez, B. Yaakobi, J. D. Zuegel, B. E. Kruschwitz, C. Dorrer, J. H. Kelly, K. U. Akli, P. K. Patel, A. J. MacKinnon, R. Betti, T. C. Sangster, and D. D. Meyerhofer, Phys. Plasmas **18**, 056703 (2011).
[27]A. Compant La Fontaine, C. Courtois, E. Lefebvre, J. L. Bourgade, O. Landoas, K. Thorp, and C. Stoeckl, Phys. Plasmas **20**, 123111 (2013).
[28]P. Choi, C. Dumitrescu, E. Wyndham, M. Favre, and H. Chuaqui, Rev. Sci. Instrum. **73**, 2276 (2002).
[29]T. A. Shelkovenko, D. B. Sinars, S. A. Pikuz, and D. A. Hammer, Phys. Plasmas **8**(4), 1305 (2001).
[30]B. R. Maddox, H. S. Park, B. A. Remington, N. Izumi, S. Chen, C. Chen, G. Kimminau, Z. Ali, M. J. Haugh, and Q. Ma, Rev. Sci. Instrum. **82**, 023111 (2011).
[31]C. Stoeckl, G. Fiksel, D. Guy, C. Mileham, P. M. Nilson, T. C. Sangster, M. J. Shoup III, and W. Theobald, Rev. Sci. Instrum. **83**, 033107 (2012).